

# Calibration and Performance of the Surface Scintillator Detector of the Pierre Auger Observatory

---

**Matteo Conte<sup>ab,\*</sup> for the Pierre Auger Collaboration<sup>c</sup>**

<sup>a</sup>*INFN Sezione di Lecce, Lecce, Italy*

<sup>b</sup>*Università del Salento, Lecce, Italy*

<sup>c</sup>*Observatorio Pierre Auger, Av. San Martín Norte 304, 5613 Malargüe, Argentina*

*Full author list:* [https://www.auger.org/archive/authors\\_icrc\\_2025.html](https://www.auger.org/archive/authors_icrc_2025.html)

*E-mail:* [spokespersons@auger.org](mailto:spokespersons@auger.org)

The Pierre Auger Observatory has led to significant advances in our understanding of ultra-high-energy cosmic rays. These new insights have driven a major upgrade of the Observatory, known as AugerPrime, through which the experiment has entered its Phase II, a new period of data collection. A key part of the upgrade is adding surface scintillator detectors (SSD) on top of the existing water-Cherenkov detectors (WCD). The main goal is to leverage their different responses to the electromagnetic and muonic shower components, enhancing the reconstruction of the primary cosmic-ray mass. In this contribution, we present the methods that involve analyzing peak and charge distributions of atmospheric muons for accurate calibration during extensive air-shower event reconstruction, along with the development of a rate-based algorithm for independent calibration. We also show the performance of the SSDs with Phase-II data, including PMT reliability and stability of key parameters, such as gain and signal-to-noise ratio.





**Figure 1:** Photograph of an open SSD at the construction phase.

## 1. Introduction

The Pierre Auger Observatory, located in Malargüe, Argentina, is the world’s largest cosmic ray detector, combining a surface array of over 1600 Water-Cherenkov Detectors (WCDs) with 27 fluorescence telescopes. Its hybrid design enables precise measurements of extensive air showers from ultra-high-energy cosmic rays (UHECRs). Over the years, the Observatory has produced key results on the energy spectrum, anisotropy, and mass composition of cosmic rays.

To enhance its capabilities, the Observatory has undergone a major upgrade – AugerPrime – which includes the addition of Surface Scintillator Detectors (SSDs) above each WCD. These detectors improve the separation of electromagnetic and muonic components, enhancing mass composition studies. In this contribution, we present the SSD calibration methods based on atmospheric muons, including a novel rate-based algorithm, and evaluate the detector performance using Phase-II data.

## 2. The Surface Scintillator Detector

The SSD module consists of two scintillator panels composed of plastic scintillator bars, encased in an aluminium box, with a photomultiplier (PMT) housed between the panels. The total active area of the scintillators in a module is  $3.84 \text{ m}^2$ . The active part of each of the scintillator panels is composed of 24 scintillator elements (bars) of 1.6 m length, 5 cm width, and 1 cm thickness. Each bar houses two horizontal holes through which wavelength-shifting (WLS) fibers are guided. The fibers are bundled and glued with optical cement in a PMMA (poly(methyl methacrylate)) cylinder, a so-called “cookie” whose front window is connected to the PMT, a bi-alkali Hamamatsu R9420, 1.5-inch diameter, with 18% quantum efficiency at a wavelength of 500 nm [1]. The picture of open SSD assembled in the laboratory is shown in Fig. 1.

The PMT is connected to the acquisition electronics, with the anode read out by a 12-bit FADC operating at 120 MHz. This results in a time binning of approximately 8.33 ns. To interpret the digital readings from the FADCs, it is necessary to define a unit that characterizes the energy deposited by minimum-ionizing particles (MIP). This approach is analogous to the one already adopted for the WCD, where signals are expressed in terms of the equivalent charge produced by vertical-centered through-going muon referred to as VEM (vertical-equivalent muon).

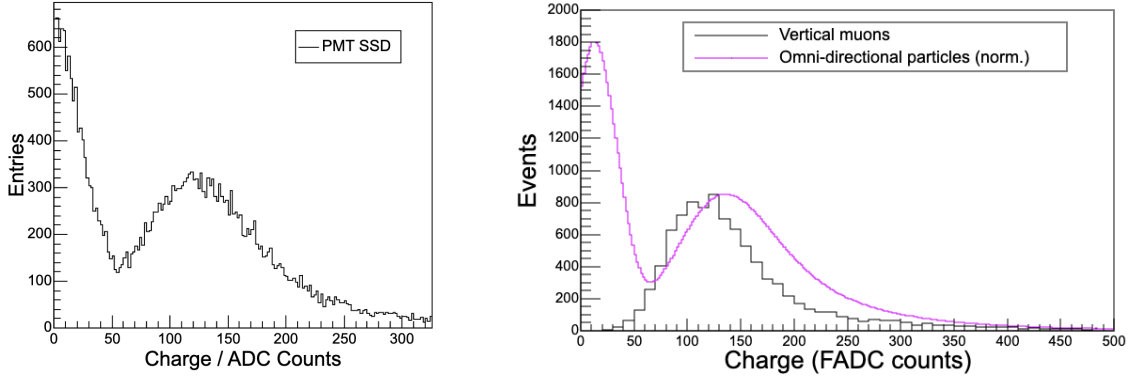


**Figure 2:** *Left:* Example of calibration histograms for the PMT of one scintilltor. *Right:* Estimation of the correction factor from omnidirectional to vertical muon distribution.

The 3 WCD and the SSD PMTs signals are divided into four high-gain and four low-gain signals, respectively. The gain ratio is set by the electronics design to 128 for the SSD channel and to 32 for the WCD PMTs [2]. This configuration extends the dynamic range above 20 000 MIP, in line with the increased dynamic range of the WCD achieved through the addition of the small PMT (see section 4.4).

### 3. Calibration methods

#### 3.1 Histogram Based Calibration

Calibration of MIP and VEM in ADC counts is based on atmospheric muons, which are abundant and energetic. For the WCD, where vertical muons cannot be isolated, charge spectra from muons arriving at all angles are continuously collected as calibration histograms.

A similar method is used for the SSD, selecting only events where a WCD PMT detects a muon-like signal, improving sample purity by exploiting the distinct response of WCD to muons and electromagnetic particles. Histograms are recorded every 61 seconds and used to estimate calibration units. An example of charge calibration histogram for the SSD is shown in the left plot of Fig. 2.

Since inclined particles deposit more energy in the SSD, a correction factor – derived from simulations and a dedicated setup using RPCs to select vertical muons – is applied to convert omnidirectional (OD) MIP values to vertical equivalents (VE), see right plot in Fig. 2. The correction factor estimated with the latter method is

$$Q_{\text{OD}}^{\text{peak}} / Q_{\text{VE}}^{\text{peak}} = 1.19 \pm 0.07, \quad (1)$$

where the quoted uncertainty of 6% is a conservative estimate, obtained by adding in quadrature the contributions from PMT instability (4%) and bar-to-bar light-yield variability (5%). Further details on the experimental setup are available in Ref. [3].

#### 3.2 Rate Based Calibration. An online estimation of the MIP Peak.

The offline calibration of the SSD detector follows the same model used for the calibration of the PMTs in the WCD, both in terms of the charge distribution (MIP Charge or  $Q_{\text{SSD}}$ ) and the

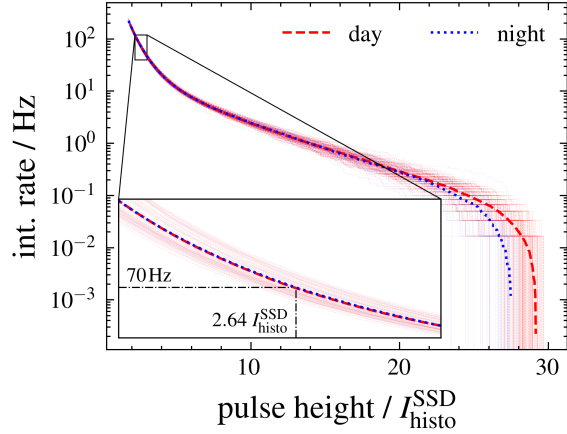


**Figure 3:** Integral rate of events with a peak height  $\geq I_{\text{SSD}}$ . The rate remains stable across day/night cycles and different local station hardware. A trigger rate of 70 Hz is achieved for a threshold of  $T_{70} = 2.64 I_{\text{SSD}}$ .

signal peak (MIP Peak or  $I_{\text{SSD}}$ ). While the WCD employs an online procedure primarily to set the detector trigger thresholds, a similar approach is not used for the scintillator. This is due to hardware limitations at the local station level and because the scintillator operates in slave mode. However, implementing an online estimate would enable real-time monitoring of the detector performance.

To this end, a rate-based model has been developed. The method employs a single-bin threshold trigger with a variable threshold  $T_{70}$ , measured in ADC counts. The number of events  $n$  in the SSD that satisfy this trigger condition is counted over an integration window  $t_{\text{cal}}$ . After each  $t_{\text{cal}}$  interval, the threshold is adjusted by a value  $\delta$ , following the steps described in details in Ref. [4]. Assuming constant electronic gain, this algorithm guarantees a stable estimate of  $T_{70}$ . To relate  $T_{70}$  to the MIP peak  $I_{\text{MIP}}$ , peak histograms are collected under the condition of a coincident signal in the WCD. The pulse height spectrum  $I$  in the SSD is measured for various stations and times of day. Using knowledge from these coincidence histograms, the pulse height spectrum is expressed in units of  $I_{\text{SSD}}^{\text{histo}}$ , and the integral event rate is calculated for thresholds of 1, 2, etc., times  $I_{\text{SSD}}^{\text{histo}}$ .

This analysis, carried out across all stations and different times of day, reveals no significant dependence on hardware or temperature. The resulting average rate-threshold relationship is shown in Fig. 3. Notably, a 70 Hz trigger rate can be achieved by applying a fixed threshold (in units of  $I_{\text{MIP}}$ ), leading to the rate-based estimator of the MIP peak  $I_{\text{SSD}}^{\text{rate}} = 2.64 T_{70}$ . It is worth noting that the 70Hz rate is currently used as a test value; further studies are ongoing to determine the optimal trigger rate for implementing an online estimator of the MIP peak.

#### 4. Performance

The Surface Scintillator Detector (SSD), part of the AugerPrime upgrade, was fully installed in 2023, with over 1400 units deployed and operational. This marked a transition phase in the data acquisition of Pierre Auger Observatory, aimed at integrating the new instruments introduced by the upgrade. Known as Phase II, this period includes all data collected with the SSDs since their deployment. This section evaluates the SSD stability based on operational parameters and early data.

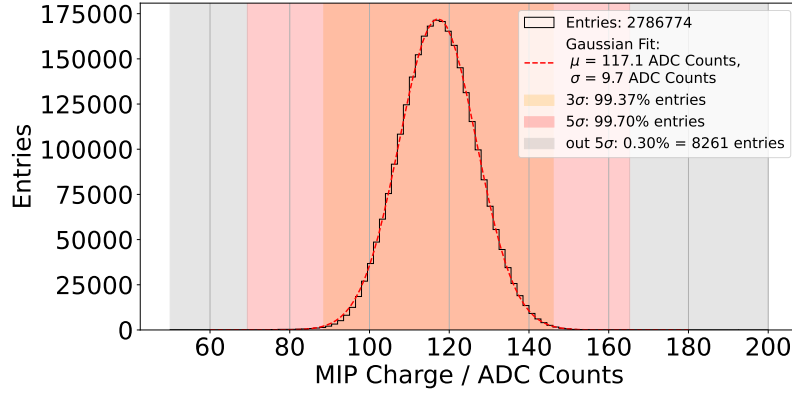


**Figure 4:** MIP charge distribution for SSD signals collected in Phase-II data.

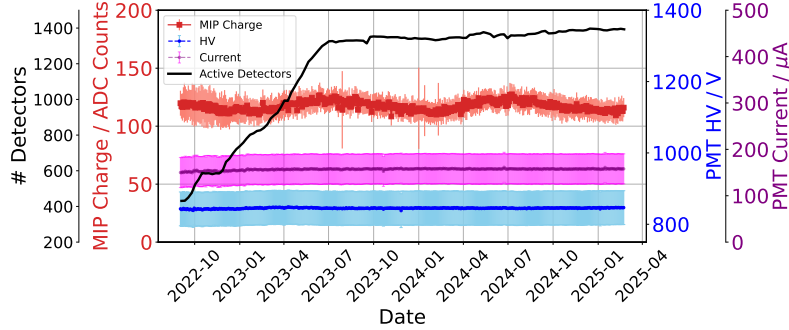


**Figure 5:** Monitoring data for HV and current for the SSD. The averages among all the detectors are showed with relative standard deviation. In red the average daily MIP charge distribution.

#### 4.1 MIP Charge Distribution

The stability of the large number of detectors deployed in the field is essential to ensure a uniform response of the SSD array. The calibration analysis performed over the first years of data shows that the distribution of the MIP charge is well described by a Gaussian, with mean and standard deviation as shown in Fig. 4. Among all calibrated signals associated with events reconstructed by the surface detector, only 0.30% fall outside a  $5\sigma$  interval from this distribution. These outliers are mainly attributed to a small subset of detectors that, for limited periods of time, operated under conditions different from the expected working point. In most cases, these deviations are associated with PMTs biased by high voltage values lying outside the typical range of 760 to 980 V.

In addition to the calibration performance, the monitoring system allows us to evaluate the long-term stability of the detector in terms of high voltage and current, as shown in Fig. 5 [5]. While the MIP charge exhibits seasonal variations – discussed in the following sections – the detector demonstrates excellent stability in terms of operating point for the active and functioning units. The plot also shows the number of detectors that were active over time, highlighting the progressive development of the array towards its full data-taking capacity in Phase II.

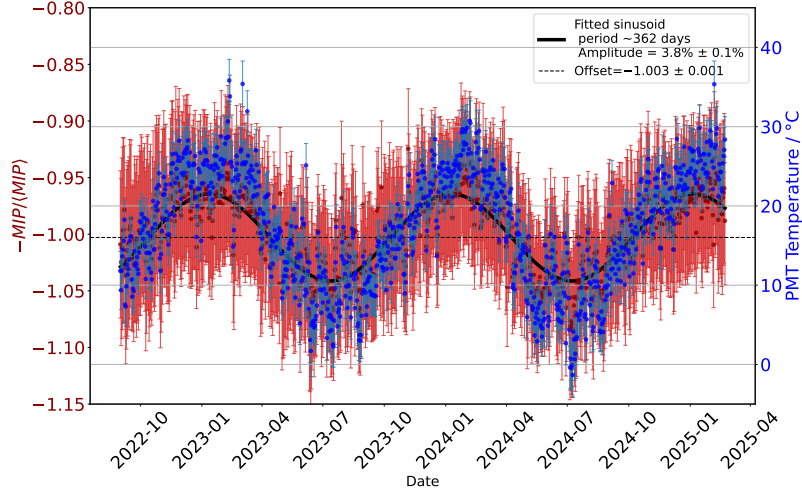


**Figure 6:** Seasonal variation of the relative MIP charge (red) and the average PMT temperature (blue).

## 4.2 Seasonal effects

The charge distribution of the photomultiplier is affected by temperature, with more stable operation observed at lower temperatures compared to higher ones. In colder conditions, the signal-to-noise ratio improves, the gain is enhanced, and the MIP charge tends to increase relative to the average level. This effect, already visible in Fig. 5, is further highlighted in Fig. 6, where a clear anti-correlation with the average PMT temperature is observed. To study the behavior of all detectors in the array over time, the MIP charge is normalized as follows:

- A dimensionless normalized MIP charge ( $mip$ ) is calculated for the  $k^{\text{th}}$  detector ( $k = 1, \dots, N_{\text{SSD}}$ ) over the full dataset as

$$mip_i^k = \left( \frac{\text{MIP}_i^k}{\text{ADC Counts}} \right) \Bigg/ \left( \frac{1}{N} \sum_{j=1}^N \frac{\text{MIP}_j^k}{\text{ADC Counts}} \right) \quad (2)$$

- A daily, array-level relative MIP charge is then defined to track collective variations,

$$\frac{\text{MIP}}{\langle \text{MIP} \rangle} (\text{day}) \equiv \frac{1}{\sum_{k=1}^{N_{\text{SSD}}} N_{\text{entries}}^k (\text{day})} \sum_{k=1}^{N_{\text{SSD}}} \sum_{i=1}^{N_{\text{entries}}^k (\text{day})} mip_i^k \quad (3)$$

The plot in Fig. 6 shows the evolution of the quantity defined in Eq. (3), inverted in sign to display the oscillation in phase with the temperature. The dominant oscillation period is found to be approximately 362 days, with an amplitude stable within about 4% on average. The uncertainty is computed as the standard deviation of the  $\text{MIP}/\langle \text{MIP} \rangle$  distribution, and accounts for detector-to-detector fluctuations as well as daily thermal variations, which will be discussed in the next section.

## 4.3 Daily temperature correlation

Following the same approach used for the seasonal analysis of the MIP charge fluctuations over time and its correlation with the daily average PMT temperature in the scintillator detectors,

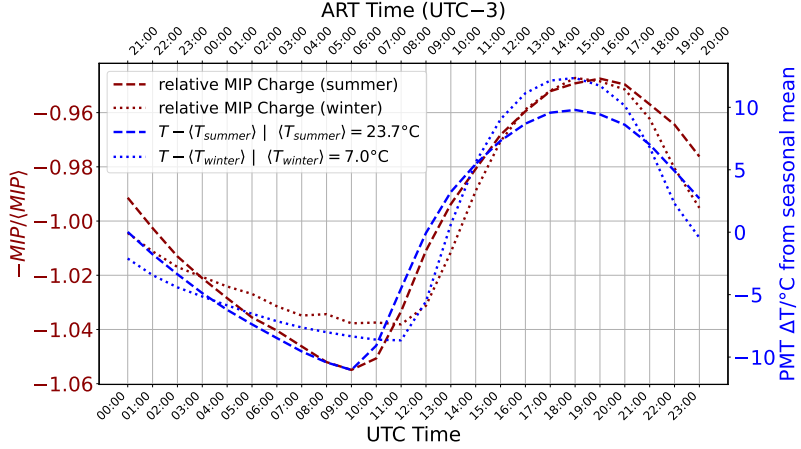


**Figure 7:** Daily variation of the MIP charge (red) and the average PMT temperature (blue), for two different periods: summer (dashed) and winter (dotted). The two horizontal axes display the time in UTC and local Argentinian time, respectively.

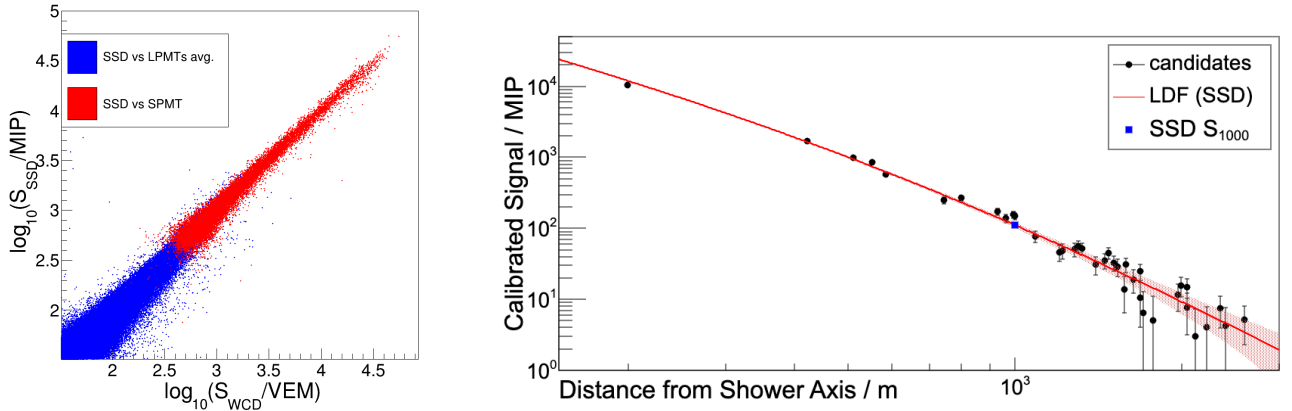


**Figure 8:** *Left:* Dynamic range. *Right:* Lateral Distribution Function fit of an SD event using the SSD signals.

this section investigates daily thermal effects by analyzing variations over the course of a day. Two periods were selected: summer (2024-12-01 to 2025-02-01) and winter (2024-07-01 to 2024-09-01). The same quantity defined in Eq. (3) is now computed hourly instead of daily.

Fig. 7 shows its evolution, plotted with inverted sign to highlight the anti-correlation with PMT temperature. The left vertical axis indicates the average PMT temperature, expressed as deviation from the seasonal mean ( $\langle T_{\text{summer}} \rangle = 23.7^\circ\text{C}$  and  $\langle T_{\text{winter}} \rangle = 7.0^\circ\text{C}$ ), to align the curves. Dashed and dotted lines represent summer and winter data, respectively.

A MIP charge variation of up to 6% is observed, with a peak-to-peak difference of  $\sim 10\%$ , more pronounced in summer. This suggests greater calibration stability during colder months, when PMTs operate at lower temperatures.

#### 4.4 Dynamic range and SSD Reconstruction

The upgrade of the surface detector stations has significantly extended the dynamic range, enhancing the ability to accurately measure signals near the shower core and reducing signal saturation. This issue was especially common in high-energy showers, where the three large PMTs (LPMTs) in the water-Cherenkov detectors often saturated.

To mitigate this, a small PMT (SPMT) was added at the center of each tank, expanding the dynamic range [6]. The scintillator detectors were similarly designed to match the SPMT range. As shown in the left panel of Fig. 8, the Phase-II configuration can handle signals up to several tens of thousands of VEM/MIP before saturation, compared to just a few thousand with LPMTs alone.

Finally, the right panel of Fig. 8 shows an event reconstructed using SSD signals. Station responses are plotted as a function of distance from the shower axis, based on the geometry from standard WCD reconstruction. The reconstructed event has a primary energy of  $E = (49.4 \pm 1.6)$  EeV and a zenith angle of  $\theta = (51.73 \pm 0.04)^\circ$ . The data are fitted with a modified NKG function, defined as

$$S(r) = S(r_{\text{opt}}) \left( \frac{r}{r_{\text{opt}}} \right)^\beta \left( \frac{r + r_s}{r_{\text{opt}} + r_s} \right)^{\beta+\gamma}. \quad (4)$$

Since the SSDs are co-located with the WCDs, the same parameters were chosen:  $r_{\text{opt}} = 1000$  m and  $r_s = 700$  m, while the parametrization of the shape parameters  $\beta$  and  $\gamma$  in terms of the shower size and zenith angle is described in Ref. [7]. As in the case of the WCD, the SSD-based reconstruction allows for the determination of a shower size parameter,  $S_{1000}$ , defined as the signal at 1000 meters from the shower core, obtained from the fit.

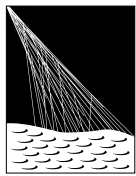
## 5. Conclusions

The installation of over 1400 SSDs as part of the AugerPrime upgrade has significantly enhanced the capabilities of Pierre Auger Observatory. We presented calibration methods based on atmospheric muons, including a rate-based approach for real-time monitoring. Performance studies show stable operation across the array, with MIP charge variations well correlated with temperature. The extended dynamic range enables accurate signal reconstruction even near the shower core. These results confirm the SSD reliability and its key role in improving mass composition analyses in Phase-II data.

## References

- [1] A. Abdul Halim *et al.* [Pierre Auger Coll.], arXiv:2507.07762.
- [2] F. Convenga *et al.* [Pierre Auger Coll.], PoS(**ICRC2023**)392.
- [3] A. Aab *et al.* [Pierre Auger Coll.], JINST **15** (2020) P09002.
- [4] P. Filip *et al.* [Pierre Auger Coll.], PoS(**UHECR2024**)085.
- [5] B. Andrada *et al.* [Pierre Auger Coll.], PoS(**ICRC2025**)176.
- [6] G.A. Anastasi *et al.* [Pierre Auger Coll.], PoS(**ICRC2023**)343.
- [7] A. Aab *et al.* [Pierre Auger Coll.], JINST **15** (2020) P10021.

## The Pierre Auger Collaboration



PIERRE  
AUGER  
OBSERVATORY

- A. Abdul Halim<sup>13</sup>, P. Abreu<sup>70</sup>, M. Aglietta<sup>53,51</sup>, I. Allekotte<sup>1</sup>, K. Almeida Cheminant<sup>78,77</sup>, A. Almela<sup>7,12</sup>, R. Aloisio<sup>44,45</sup>, J. Alvarez-Muñiz<sup>76</sup>, A. Ambrosone<sup>44</sup>, J. Ammerman Yebra<sup>76</sup>, G.A. Anastasi<sup>57,46</sup>, L. Anchordoqui<sup>83</sup>, B. Andrade<sup>7</sup>, L. Andrade Dourado<sup>44,45</sup>, S. Andringa<sup>70</sup>, L. Apollonio<sup>58,48</sup>, C. Aramo<sup>49</sup>, E. Arnone<sup>62,51</sup>, J.C. Arteaga Velázquez<sup>66</sup>, P. Assis<sup>70</sup>, G. Avila<sup>11</sup>, E. Avocone<sup>56,45</sup>, A. Bakalova<sup>31</sup>, F. Barbato<sup>44,45</sup>, A. Bartz Mocellin<sup>82</sup>, J.A. Bellido<sup>13</sup>, C. Berat<sup>35</sup>, M.E. Bertaina<sup>62,51</sup>, M. Bianciotto<sup>62,51</sup>, P.L. Biermann<sup>a</sup>, V. Binet<sup>5</sup>, K. Bismarck<sup>38,7</sup>, T. Bister<sup>77,78</sup>, J. Biteau<sup>36,i</sup>, J. Blazek<sup>31</sup>, J. Blümner<sup>40</sup>, M. Boháčová<sup>31</sup>, D. Boncioli<sup>56,45</sup>, C. Bonifazi<sup>8</sup>, L. Bonneau Arbeletche<sup>22</sup>, N. Borodai<sup>68</sup>, J. Brack<sup>f</sup>, P.G. Brichetto Orcher<sup>7,40</sup>, F.L. Briechle<sup>41</sup>, A. Bueno<sup>75</sup>, S. Buitink<sup>15</sup>, M. Buscemi<sup>46,57</sup>, M. Büskens<sup>38,7</sup>, A. Bwembya<sup>77,78</sup>, K.S. Caballero-Mora<sup>65</sup>, S. Cabana-Freire<sup>76</sup>, L. Caccianiga<sup>58,48</sup>, F. Campuzano<sup>6</sup>, J. Caraça-Valente<sup>82</sup>, R. Caruso<sup>57,46</sup>, A. Castellina<sup>53,51</sup>, F. Catalani<sup>19</sup>, G. Cataldi<sup>47</sup>, L. Cazon<sup>76</sup>, M. Cerda<sup>10</sup>, B. Čermáková<sup>40</sup>, A. Cermenati<sup>44,45</sup>, J.A. Chinellato<sup>22</sup>, J. Chudoba<sup>31</sup>, L. Chytha<sup>32</sup>, R.W. Clay<sup>13</sup>, A.C. Cobos Cerutti<sup>6</sup>, R. Colalillo<sup>59,49</sup>, R. Conceição<sup>70</sup>, G. Consolati<sup>48,54</sup>, M. Conte<sup>55,47</sup>, F. Convenga<sup>44,45</sup>, D. Correia dos Santos<sup>27</sup>, P.J. Costa<sup>70</sup>, C.E. Covault<sup>81</sup>, M. Cristinziani<sup>43</sup>, C.S. Cruz Sanchez<sup>3</sup>, S. Dasso<sup>4,2</sup>, K. Daumiller<sup>40</sup>, B.R. Dawson<sup>13</sup>, R.M. de Almeida<sup>27</sup>, E.-T. de Boone<sup>43</sup>, B. de Errico<sup>27</sup>, J. de Jesús<sup>7</sup>, S.J. de Jong<sup>77,78</sup>, J.R.T. de Mello Neto<sup>27</sup>, I. De Mitri<sup>44,45</sup>, J. de Oliveira<sup>18</sup>, D. de Oliveira Franco<sup>42</sup>, F. de Palma<sup>55,47</sup>, V. de Souza<sup>20</sup>, E. De Vito<sup>55,47</sup>, A. Del Popolo<sup>57,46</sup>, O. Deligny<sup>33</sup>, N. Denner<sup>31</sup>, L. Deval<sup>53,51</sup>, A. di Matteo<sup>51</sup>, C. Dobrigkeit<sup>22</sup>, J.C. D'Olivo<sup>67</sup>, L.M. Domingues Mendes<sup>16,70</sup>, Q. Dorost<sup>43</sup>, J.C. dos Anjos<sup>16</sup>, R.C. dos Anjos<sup>26</sup>, J. Ebr<sup>31</sup>, F. Ellwanger<sup>40</sup>, R. Engel<sup>38,40</sup>, I. Epicoco<sup>55,47</sup>, M. Erdmann<sup>41</sup>, A. Etchegoyen<sup>7,12</sup>, C. Evoli<sup>44,45</sup>, H. Falcke<sup>77,79,78</sup>, G. Farrar<sup>85</sup>, A.C. Fauth<sup>22</sup>, T. Fehler<sup>43</sup>, F. Feldbusch<sup>39</sup>, A. Fernandes<sup>70</sup>, M. Fernandez<sup>14</sup>, B. Fick<sup>84</sup>, J.M. Figueira<sup>7</sup>, P. Filip<sup>38,7</sup>, A. Filipčič<sup>74,73</sup>, T. Fitoussi<sup>40</sup>, B. Flagg<sup>87</sup>, T. Fodran<sup>77</sup>, A. Franco<sup>47</sup>, M. Freitas<sup>70</sup>, T. Fujii<sup>86,h</sup>, A. Fuster<sup>7,12</sup>, C. Galea<sup>77</sup>, B. García<sup>6</sup>, C. Gaudí<sup>37</sup>, P.L. Ghia<sup>33</sup>, U. Giaccari<sup>47</sup>, F. Gobbi<sup>10</sup>, F. Gollan<sup>7</sup>, G. Golup<sup>1</sup>, M. Gómez Berisso<sup>1</sup>, P.F. Gómez Vitale<sup>11</sup>, J.P. Gongora<sup>11</sup>, J.M. González<sup>1</sup>, N. González<sup>7</sup>, D. Góra<sup>68</sup>, A. Gorgi<sup>53,51</sup>, M. Gottowik<sup>40</sup>, F. Guarino<sup>59,49</sup>, G.P. Guedes<sup>23</sup>, L. Gülow<sup>40</sup>, S. Hahn<sup>38</sup>, P. Hamal<sup>31</sup>, M.R. Hampel<sup>7</sup>, P. Hansen<sup>3</sup>, V.M. Harvey<sup>13</sup>, A. Haungs<sup>40</sup>, T. Hebbeker<sup>41</sup>, C. Hojvat<sup>d</sup>, J.R. Hörandel<sup>77,78</sup>, P. Horvath<sup>32</sup>, M. Hrabovsky<sup>32</sup>, T. Huege<sup>40,15</sup>, A. Insolia<sup>57,46</sup>, P.G. Isar<sup>72</sup>, M. Ismaiel<sup>77,78</sup>, P. Janecek<sup>31</sup>, V. Jilek<sup>31</sup>, K.-H. Kampert<sup>37</sup>, B. Keilhauer<sup>40</sup>, A. Khakurdi<sup>77</sup>, V.V. Kizakke Covilakam<sup>7,40</sup>, H.O. Klages<sup>40</sup>, M. Kleifges<sup>39</sup>, J. Köhler<sup>40</sup>, F. Krieger<sup>41</sup>, M. Kubatova<sup>31</sup>, N. Kunka<sup>39</sup>, B.L. Lago<sup>17</sup>, N. Langner<sup>41</sup>, N. Leal<sup>7</sup>, M.A. Leigui de Oliveira<sup>25</sup>, Y. Lema-Capeans<sup>76</sup>, A. Letessier-Selvon<sup>34</sup>, I. Lhenry-Yvon<sup>33</sup>, L. Lopes<sup>70</sup>, J.P. Lundquist<sup>73</sup>, M. Mallamaci<sup>60,46</sup>, D. Mandat<sup>31</sup>, P. Mantsch<sup>d</sup>, F.M. Mariani<sup>58,48</sup>, A.G. Mariazzi<sup>3</sup>, I.C. Marić<sup>14</sup>, G. Marsella<sup>60,46</sup>, D. Martello<sup>55,47</sup>, S. Martinelli<sup>40,7</sup>, M.A. Martins<sup>76</sup>, H.-J. Mathes<sup>40</sup>, J. Matthews<sup>g</sup>, G. Matthiae<sup>61,50</sup>, E. Mayotte<sup>82</sup>, S. Mayotte<sup>82</sup>, P.O. Mazur<sup>d</sup>, G. Medina-Tanco<sup>67</sup>, J. Meinert<sup>37</sup>, D. Melo<sup>7</sup>, A. Menshikov<sup>39</sup>, C. Merx<sup>40</sup>, S. Michal<sup>31</sup>, M.I. Micheletti<sup>5</sup>, L. Miramonti<sup>58,48</sup>, M. Mogarkar<sup>68</sup>, S. Mollerach<sup>1</sup>, F. Montanet<sup>35</sup>, L. Morejon<sup>37</sup>, K. Mulrey<sup>77,78</sup>, R. Mussa<sup>51</sup>, W.M. Namasaka<sup>37</sup>, S. Negi<sup>31</sup>, L. Nellen<sup>67</sup>, K. Nguyen<sup>84</sup>, G. Nicora<sup>9</sup>, M. Niechciol<sup>43</sup>, D. Nitz<sup>84</sup>, D. Nosek<sup>30</sup>, A. Novikov<sup>87</sup>, V. Novotny<sup>30</sup>, L. Nožka<sup>32</sup>, A. Nucita<sup>55,47</sup>, L.A. Núñez<sup>29</sup>, J. Ochoa<sup>7,40</sup>, C. Oliveira<sup>20</sup>, L. Östman<sup>31</sup>, M. Palatka<sup>31</sup>, J. Pallotta<sup>9</sup>, S. Panja<sup>31</sup>, G. Parente<sup>76</sup>, T. Paulsen<sup>37</sup>, J. Pawlowsky<sup>37</sup>, M. Pech<sup>31</sup>, J. Pěkala<sup>68</sup>, R. Pelayo<sup>64</sup>, V. Pelgrims<sup>14</sup>, L.A.S. Pereira<sup>24</sup>, E.E. Pereira Martins<sup>38,7</sup>, C. Pérez Bertolli<sup>7,40</sup>, L. Perrone<sup>55,47</sup>, S. Petrera<sup>44,45</sup>, C. Petrucci<sup>56</sup>, T. Pierog<sup>40</sup>, M. Pimenta<sup>70</sup>, M. Platino<sup>7</sup>, B. Pont<sup>77</sup>, M. Pourmohammad Shahvar<sup>60,46</sup>, P. Privitera<sup>86</sup>, C. Priyatadarsi<sup>68</sup>, M. Prouza<sup>31</sup>, K. Pytel<sup>69</sup>, S. Querchfeld<sup>37</sup>, J. Rautenberg<sup>37</sup>, D. Ravignani<sup>7</sup>, J.V. Reginatto Akim<sup>22</sup>, A. Reuzki<sup>41</sup>, J. Ridky<sup>31</sup>, F. Riehn<sup>76,j</sup>, M. Risse<sup>43</sup>, V. Rizi<sup>56,45</sup>, E. Rodriguez<sup>7,40</sup>, G. Rodriguez Fernandez<sup>50</sup>, J. Rodriguez Rojo<sup>11</sup>, S. Rossoni<sup>42</sup>, M. Roth<sup>40</sup>, E. Roulet<sup>1</sup>, A.C. Rovero<sup>4</sup>, A. Saftoiu<sup>71</sup>, M. Saharan<sup>77</sup>, F. Salamida<sup>56,45</sup>, H. Salazar<sup>63</sup>, G. Salina<sup>50</sup>, P. Sampathkumar<sup>40</sup>, N. San Martin<sup>82</sup>, J.D. Sanabria Gomez<sup>29</sup>, F. Sánchez<sup>7</sup>, E.M. Santos<sup>21</sup>, E. Santos<sup>31</sup>, F. Sarazin<sup>82</sup>, R. Sarmento<sup>70</sup>, R. Sato<sup>11</sup>, P. Savina<sup>44,45</sup>, V. Scherini<sup>55,47</sup>, H. Schieler<sup>40</sup>, M. Schimassek<sup>33</sup>, M. Schimp<sup>37</sup>, D. Schmidt<sup>40</sup>, O. Scholten<sup>15,b</sup>, H. Schoorlemmer<sup>77,78</sup>, P. Schovánek<sup>31</sup>, F.G. Schröder<sup>87,40</sup>, J. Schulz<sup>41</sup>, T. Schulz<sup>31</sup>, S.J. Sciutto<sup>3</sup>, M. Scornavacche<sup>7</sup>, A. Sedoski<sup>7</sup>, A. Segreto<sup>52,46</sup>, S. Sehgal<sup>37</sup>, S.U. Shivashankara<sup>73</sup>, G. Sigl<sup>42</sup>, K. Simkova<sup>15,14</sup>, F. Simon<sup>39</sup>, R. Šmídá<sup>86</sup>, P. Sommers<sup>e</sup>, R. Squartini<sup>10</sup>, M. Stadelmaier<sup>40,48,58</sup>, S. Stanić<sup>73</sup>, J. Stasielak<sup>68</sup>, P. Stassi<sup>35</sup>, S. Strähn<sup>38</sup>, M. Straub<sup>41</sup>, T. Suomijärvi<sup>36</sup>, A.D. Supanitsky<sup>7</sup>, Z. Svozilikova<sup>31</sup>, K. Syrokvas<sup>30</sup>, Z. Szadkowski<sup>69</sup>, F. Tairli<sup>13</sup>, M. Tambone<sup>59,49</sup>, A. Tapia<sup>28</sup>, C. Taricco<sup>62,51</sup>, C. Timmermans<sup>78,77</sup>, O. Tkachenko<sup>31</sup>, P. Tobiska<sup>31</sup>, C.J. Todero Peixoto<sup>19</sup>, B. Tomé<sup>70</sup>, A. Travaini<sup>10</sup>, P. Travnicek<sup>31</sup>, M. Tueros<sup>3</sup>, M. Unger<sup>40</sup>, R. Uzeiroska<sup>37</sup>, L. Vaclavek<sup>32</sup>, M. Vacula<sup>32</sup>, I. Vaiman<sup>44,45</sup>, J.F. Valdés Galicia<sup>67</sup>, L. Valore<sup>59,49</sup>, P. van Dillen<sup>77,78</sup>, E. Varela<sup>63</sup>, V. Vašíčková<sup>37</sup>, A. Vásquez-Ramírez<sup>29</sup>, D. Veberič<sup>40</sup>, I.D. Vergara Quispe<sup>3</sup>, S. Verpoest<sup>87</sup>, V. Verzi<sup>50</sup>, J. Vicha<sup>31</sup>, J. Vink<sup>80</sup>, S. Vorobiov<sup>73</sup>, J.B. Vuta<sup>31</sup>, C. Watanabe<sup>27</sup>, A.A. Watson<sup>c</sup>, A. Weindl<sup>40</sup>, M. Weitz<sup>37</sup>, L. Wiencke<sup>82</sup>, H. Wilczyński<sup>68</sup>, B. Wundheiler<sup>7</sup>, B. Yue<sup>37</sup>, A. Yushkov<sup>31</sup>, E. Zas<sup>76</sup>, D. Zavrtanik<sup>73,74</sup>, M. Zavrtanik<sup>74,73</sup>

- <sup>1</sup> Centro Atómico Bariloche and Instituto Balseiro (CNEA-UNCuyo-CONICET), San Carlos de Bariloche, Argentina  
<sup>2</sup> Departamento de Física and Departamento de Ciencias de la Atmósfera y los Océanos, FCEyN, Universidad de Buenos Aires and CONICET, Buenos Aires, Argentina  
<sup>3</sup> IFLP, Universidad Nacional de La Plata and CONICET, La Plata, Argentina  
<sup>4</sup> Instituto de Astronomía y Física del Espacio (IAFE, CONICET-UBA), Buenos Aires, Argentina  
<sup>5</sup> Instituto de Física de Rosario (IFIR) – CONICET/U.N.R. and Facultad de Ciencias Bioquímicas y Farmacéuticas U.N.R., Rosario, Argentina  
<sup>6</sup> Instituto de Tecnologías en Detección y Astropartículas (CNEA, CONICET, UNSAM), and Universidad Tecnológica Nacional – Facultad Regional Mendoza (CONICET/CNEA), Mendoza, Argentina  
<sup>7</sup> Instituto de Tecnologías en Detección y Astropartículas (CNEA, CONICET, UNSAM), Buenos Aires, Argentina  
<sup>8</sup> International Center of Advanced Studies and Instituto de Ciencias Físicas, ECyT-UNSAM and CONICET, Campus Miguelete – San Martín, Buenos Aires, Argentina  
<sup>9</sup> Laboratorio Atmósfera – Departamento de Investigaciones en Láseres y sus Aplicaciones – UNIDEF (CITEDEF-CONICET), Argentina  
<sup>10</sup> Observatorio Pierre Auger, Malargüe, Argentina  
<sup>11</sup> Observatorio Pierre Auger and Comisión Nacional de Energía Atómica, Malargüe, Argentina  
<sup>12</sup> Universidad Tecnológica Nacional – Facultad Regional Buenos Aires, Buenos Aires, Argentina  
<sup>13</sup> University of Adelaide, Adelaide, S.A., Australia  
<sup>14</sup> Université Libre de Bruxelles (ULB), Brussels, Belgium  
<sup>15</sup> Vrije Universiteit Brussels, Brussels, Belgium  
<sup>16</sup> Centro Brasileiro de Pesquisas Fisicas, Rio de Janeiro, RJ, Brazil  
<sup>17</sup> Centro Federal de Educação Tecnológica Celso Suckow da Fonseca, Petropolis, Brazil  
<sup>18</sup> Instituto Federal de Educação, Ciência e Tecnologia do Rio de Janeiro (IFRJ), Brazil  
<sup>19</sup> Universidade de São Paulo, Escola de Engenharia de Lorena, Lorena, SP, Brazil  
<sup>20</sup> Universidade de São Paulo, Instituto de Física de São Carlos, São Carlos, SP, Brazil  
<sup>21</sup> Universidade de São Paulo, Instituto de Física, São Paulo, SP, Brazil  
<sup>22</sup> Universidade Estadual de Campinas (UNICAMP), IFGW, Campinas, SP, Brazil  
<sup>23</sup> Universidade Estadual de Feira de Santana, Feira de Santana, Brazil  
<sup>24</sup> Universidade Federal de Campina Grande, Centro de Ciencias e Tecnologia, Campina Grande, Brazil  
<sup>25</sup> Universidade Federal do ABC, Santo André, SP, Brazil  
<sup>26</sup> Universidade Federal do Paraná, Setor Palotina, Palotina, Brazil  
<sup>27</sup> Universidade Federal do Rio de Janeiro, Instituto de Física, Rio de Janeiro, RJ, Brazil  
<sup>28</sup> Universidad de Medellín, Medellín, Colombia  
<sup>29</sup> Universidad Industrial de Santander, Bucaramanga, Colombia  
<sup>30</sup> Charles University, Faculty of Mathematics and Physics, Institute of Particle and Nuclear Physics, Prague, Czech Republic  
<sup>31</sup> Institute of Physics of the Czech Academy of Sciences, Prague, Czech Republic  
<sup>32</sup> Palacky University, Olomouc, Czech Republic  
<sup>33</sup> CNRS/IN2P3, IJCLab, Université Paris-Saclay, Orsay, France  
<sup>34</sup> Laboratoire de Physique Nucléaire et de Hautes Energies (LPNHE), Sorbonne Université, Université de Paris, CNRS-IN2P3, Paris, France  
<sup>35</sup> Univ. Grenoble Alpes, CNRS, Grenoble Institute of Engineering Univ. Grenoble Alpes, LPSC-IN2P3, 38000 Grenoble, France  
<sup>36</sup> Université Paris-Saclay, CNRS/IN2P3, IJCLab, Orsay, France  
<sup>37</sup> Bergische Universität Wuppertal, Department of Physics, Wuppertal, Germany  
<sup>38</sup> Karlsruhe Institute of Technology (KIT), Institute for Experimental Particle Physics, Karlsruhe, Germany  
<sup>39</sup> Karlsruhe Institute of Technology (KIT), Institut für Prozessdatenverarbeitung und Elektronik, Karlsruhe, Germany  
<sup>40</sup> Karlsruhe Institute of Technology (KIT), Institute for Astroparticle Physics, Karlsruhe, Germany  
<sup>41</sup> RWTH Aachen University, III. Physikalischs Institut A, Aachen, Germany  
<sup>42</sup> Universität Hamburg, II. Institut für Theoretische Physik, Hamburg, Germany  
<sup>43</sup> Universität Siegen, Department Physik – Experimentelle Teilchenphysik, Siegen, Germany  
<sup>44</sup> Gran Sasso Science Institute, L'Aquila, Italy  
<sup>45</sup> INFN Laboratori Nazionali del Gran Sasso, Assergi (L'Aquila), Italy  
<sup>46</sup> INFN, Sezione di Catania, Catania, Italy  
<sup>47</sup> INFN, Sezione di Lecce, Lecce, Italy  
<sup>48</sup> INFN, Sezione di Milano, Milano, Italy  
<sup>49</sup> INFN, Sezione di Napoli, Napoli, Italy  
<sup>50</sup> INFN, Sezione di Roma "Tor Vergata", Roma, Italy  
<sup>51</sup> INFN, Sezione di Torino, Torino, Italy

- <sup>52</sup> Istituto di Astrofisica Spaziale e Fisica Cosmica di Palermo (INAF), Palermo, Italy  
<sup>53</sup> Osservatorio Astrofisico di Torino (INAF), Torino, Italy  
<sup>54</sup> Politecnico di Milano, Dipartimento di Scienze e Tecnologie Aerospaziali , Milano, Italy  
<sup>55</sup> Università del Salento, Dipartimento di Matematica e Fisica "E. De Giorgi", Lecce, Italy  
<sup>56</sup> Università dell'Aquila, Dipartimento di Scienze Fisiche e Chimiche, L'Aquila, Italy  
<sup>57</sup> Università di Catania, Dipartimento di Fisica e Astronomia "Ettore Majorana", Catania, Italy  
<sup>58</sup> Università di Milano, Dipartimento di Fisica, Milano, Italy  
<sup>59</sup> Università di Napoli "Federico II", Dipartimento di Fisica "Ettore Pancini", Napoli, Italy  
<sup>60</sup> Università di Palermo, Dipartimento di Fisica e Chimica "E. Segrè", Palermo, Italy  
<sup>61</sup> Università di Roma "Tor Vergata", Dipartimento di Fisica, Roma, Italy  
<sup>62</sup> Università Torino, Dipartimento di Fisica, Torino, Italy  
<sup>63</sup> Benemérita Universidad Autónoma de Puebla, Puebla, México  
<sup>64</sup> Unidad Profesional Interdisciplinaria en Ingeniería y Tecnologías Avanzadas del Instituto Politécnico Nacional (UPIITA-IPN), México, D.F., México  
<sup>65</sup> Universidad Autónoma de Chiapas, Tuxtla Gutiérrez, Chiapas, México  
<sup>66</sup> Universidad Michoacana de San Nicolás de Hidalgo, Morelia, Michoacán, México  
<sup>67</sup> Universidad Nacional Autónoma de México, México, D.F., México  
<sup>68</sup> Institute of Nuclear Physics PAN, Krakow, Poland  
<sup>69</sup> University of Łódź, Faculty of High-Energy Astrophysics, Łódź, Poland  
<sup>70</sup> Laboratório de Instrumentação e Física Experimental de Partículas – LIP and Instituto Superior Técnico – IST, Universidade de Lisboa – UL, Lisboa, Portugal  
<sup>71</sup> "Horia Hulubei" National Institute for Physics and Nuclear Engineering, Bucharest-Magurele, Romania  
<sup>72</sup> Institute of Space Science, Bucharest-Magurele, Romania  
<sup>73</sup> Center for Astrophysics and Cosmology (CAC), University of Nova Gorica, Nova Gorica, Slovenia  
<sup>74</sup> Experimental Particle Physics Department, J. Stefan Institute, Ljubljana, Slovenia  
<sup>75</sup> Universidad de Granada and C.A.F.P.E., Granada, Spain  
<sup>76</sup> Instituto Galego de Física de Altas Enerxías (IGFAE), Universidade de Santiago de Compostela, Santiago de Compostela, Spain  
<sup>77</sup> IMAPP, Radboud University Nijmegen, Nijmegen, The Netherlands  
<sup>78</sup> Nationaal Instituut voor Kernfysica en Hoge Energie Fysica (NIKHEF), Science Park, Amsterdam, The Netherlands  
<sup>79</sup> Stichting Astronomisch Onderzoek in Nederland (ASTRON), Dwingeloo, The Netherlands  
<sup>80</sup> Universiteit van Amsterdam, Faculty of Science, Amsterdam, The Netherlands  
<sup>81</sup> Case Western Reserve University, Cleveland, OH, USA  
<sup>82</sup> Colorado School of Mines, Golden, CO, USA  
<sup>83</sup> Department of Physics and Astronomy, Lehman College, City University of New York, Bronx, NY, USA  
<sup>84</sup> Michigan Technological University, Houghton, MI, USA  
<sup>85</sup> New York University, New York, NY, USA  
<sup>86</sup> University of Chicago, Enrico Fermi Institute, Chicago, IL, USA  
<sup>87</sup> University of Delaware, Department of Physics and Astronomy, Bartol Research Institute, Newark, DE, USA

<sup>a</sup> Max-Planck-Institut für Radioastronomie, Bonn, Germany<sup>b</sup> also at Kapteyn Institute, University of Groningen, Groningen, The Netherlands<sup>c</sup> School of Physics and Astronomy, University of Leeds, Leeds, United Kingdom<sup>d</sup> Fermi National Accelerator Laboratory, Fermilab, Batavia, IL, USA<sup>e</sup> Pennsylvania State University, University Park, PA, USA<sup>f</sup> Colorado State University, Fort Collins, CO, USA<sup>g</sup> Louisiana State University, Baton Rouge, LA, USA<sup>h</sup> now at Graduate School of Science, Osaka Metropolitan University, Osaka, Japan<sup>i</sup> Institut universitaire de France (IUF), France<sup>j</sup> now at Technische Universität Dortmund and Ruhr-Universität Bochum, Dortmund and Bochum, Germany

## Acknowledgments

The successful installation, commissioning, and operation of the Pierre Auger Observatory would not have been possible without the strong commitment and effort from the technical and administrative staff in Malargüe. We are very grateful to the following agencies and organizations for financial support:

Argentina – Comisión Nacional de Energía Atómica; Agencia Nacional de Promoción Científica y Tecnológica (ANPCyT); Consejo Nacional de Investigaciones Científicas y Técnicas (CONICET); Gobierno de la Provincia de

Mendoza; Municipalidad de Malargüe; NDM Holdings and Valle Las Leñas; in gratitude for their continuing cooperation over land access; Australia – the Australian Research Council; Belgium – Fonds de la Recherche Scientifique (FNRS); Research Foundation Flanders (FWO), Marie Curie Action of the European Union Grant No. 101107047; Brazil – Conselho Nacional de Desenvolvimento Científico e Tecnológico (CNPq); Financiadora de Estudos e Projetos (FINEP); Fundação de Amparo à Pesquisa do Estado de Rio de Janeiro (FAPERJ); São Paulo Research Foundation (FAPESP) Grants No. 2019/10151-2, No. 2010/07359-6 and No. 1999/05404-3; Ministério da Ciência, Tecnologia, Inovações e Comunicações (MCTIC); Czech Republic – GACR 24-13049S, CAS LQ100102401, MEYS LM2023032, CZ.02.1.01/0.0/0.0/16\_013/0001402, CZ.02.1.01/0.0/0.0/18\_046/0016010 and CZ.02.1.01/0.0/0.0/17\_049/0008422 and CZ.02.01.01/00/22\_008/0004632; France – Centre de Calcul IN2P3/CNRS; Centre National de la Recherche Scientifique (CNRS); Conseil Régional Ile-de-France; Département Physique Nucléaire et Corpusculaire (PNC-IN2P3/CNRS); Département Sciences de l'Univers (SDU-INSU/CNRS); Institut Lagrange de Paris (ILP) Grant No. LABEX ANR-10-LABX-63 within the Investissements d'Avenir Programme Grant No. ANR-11-IDEX-0004-02; Germany – Bundesministerium für Bildung und Forschung (BMBF); Deutsche Forschungsgemeinschaft (DFG); Finanzministerium Baden-Württemberg; Helmholtz Alliance for Astroparticle Physics (HAP); Helmholtz-Gemeinschaft Deutscher Forschungszentren (HGF); Ministerium für Kultur und Wissenschaft des Landes Nordrhein-Westfalen; Ministerium für Wissenschaft, Forschung und Kunst des Landes Baden-Württemberg; Italy – Istituto Nazionale di Fisica Nucleare (INFN); Istituto Nazionale di Astrofisica (INAF); Ministero dell'Università e della Ricerca (MUR); CETEMPS Center of Excellence; Ministero degli Affari Esteri (MAE), ICSC Centro Nazionale di Ricerca in High Performance Computing, Big Data and Quantum Computing, funded by European Union NextGenerationEU, reference code CN\_00000013; México – Consejo Nacional de Ciencia y Tecnología (CONACYT) No. 167733; Universidad Nacional Autónoma de México (UNAM); PAPIIT DGAPA-UNAM; The Netherlands – Ministry of Education, Culture and Science; Netherlands Organisation for Scientific Research (NWO); Dutch national e-infrastructure with the support of SURF Cooperative; Poland – Ministry of Education and Science, grants No. DIR/WK/2018/11 and 2022/WK/12; National Science Centre, grants No. 2016/22/M/ST9/00198, 2016/23/B/ST9/01635, 2020/39/B/ST9/01398, and 2022/45/B/ST9/02163; Portugal – Portuguese national funds and FEDER funds within Programa Operacional Factores de Competitividade through Fundação para a Ciéncia e a Tecnologia (COMPETE); Romania – Ministry of Research, Innovation and Digitization, CNCS-UEFISCDI, contract no. 30N/2023 under Romanian National Core Program LAPLAS VII, grant no. PN 23 21 01 02 and project number PN-III-P1-1.1-TE-2021-0924/TE57/2022, within PNCDI III; Slovenia – Slovenian Research Agency, grants P1-0031, P1-0385, I0-0033, NI-0111; Spain – Ministerio de Ciencia e Innovación/Agenzia Estatal de Investigación (PID2019-105544GB-I00, PID2022-140510NB-I00 and RYC2019-027017-I), Xunta de Galicia (CIGUS Network of Research Centers, Consolidación 2021 GRC GI-2033, ED431C-2021/22 and ED431F-2022/15), Junta de Andalucía (SOMM17/6104/UGR and P18-FR-4314), and the European Union (Marie Skłodowska-Curie 101065027 and ERDF); USA – Department of Energy, Contracts No. DE-AC02-07CH11359, No. DE-FR02-04ER41300, No. DE-FG02-99ER41107 and No. DE-SC0011689; National Science Foundation, Grant No. 0450696, and NSF-2013199; The Grainger Foundation; Marie Curie-IRSES/EPLANET; European Particle Physics Latin American Network; and UNESCO.